International Journal of Pressure Vessels and Piping 214 (2025) 105434

Contents lists available at ScienceDirect

International Journal of Pressure Vessels and Piping

journal homepage: www.elsevier.com/locate/ijpvp

Post weld heat treatment of bisalloy 80 steel: Mechanics and industry safety code compatibility

Houman Alipooramirabad [a,*], Anna Paradowska [b,c], Mark Reid [b], Reza Ghomashchi [d]

[a] College of Engineering, Birmingham City University, Birmingham, UK
[b] Australian Nuclear Science and Technology Organisation (ANSTO), Sydney, Australia
[c] School of Civil Engineering, The University of Sydney, Sydney, Australia
[d] School of Mechanical & Electrical Engineering, The University of Adelaide, Adelaide, Australia

ABSTRACT

The present study utilized both in-situ and ex-situ neutron diffraction to evaluate the evolution of residual strains/stresses before, during and after Post-Weld Heat Treatment (PWHT) of quenched and tempered (Q&T) Bisalloy 80 steel welded by pulsed Gas Metal Arc Welding (GMAW-P). It was found that strain/stress relaxation mainly occurred during the reheating step with a high relaxation rate and steep slope (~67 % of strain relaxation) while linear strain relief was observed during holding (soaking) time. Most of the strain relief occurred within the temperature range of 450°C–600 °C which is believed to be due to creep strain development occurring far earlier than the component reaching the isothermal holding temperature. The ex-situ neutron diffraction measurements were similar to in-situ results confirming the applied PWHT effectively mitigated the residual stresses (the maximum longitudinal stress reduced to around 23 % of the weld metal yield strength).

The measurements were compared with existing literature data and the current fitness of safety assessment codes (BS7910 and R6). It was found that both assessment codes were conservative for both the transverse and longitudinal residual stresses in the region close to the weld toe. Furthermore, both standards may underestimate through-thickness residual stresses in the transverse direction.

1. Introduction

Q&T steels have numerous uses in engineering; from structural and wear-resistant requirements like mining [1] to armoured vehicles manufactured for defence force [2,3]. The exceptional features of high hardness and superior toughness of Q&T steels coupled with better weldability make them an ideal material for unconventional applications having complex loading patterns including high strain rates, as experienced with the ballistic projectiles impacts or explosive blasts [4–6]. Despite the improved weldability of these alloys, there are still challenges encountered during welding such as softening of the heat affected zone (HAZ) or generation of high tensile residual stresses. These effects could potentially threaten the structural integrity of welded components, especially in the presence of severe environmental conditions, or under loading regime with potential creep/fatigue failure [7–11]. Aggressive environments may lead to stress corrosion cracking-SCC, hydrogen induced cracking-HIC, fatigue or combined fatigue and creep cracking. All these could result in crack development and component failure at lower operating stresses than expected [4,10,12,13]. There is, therefore, a need to evaluate the residual stresses developed during welding of high-strength steel structural components, and the efficacy of stress mitigation techniques, in particularly PWHT. often applied to relieve the high tensile residual stresses in the weldments.

PWHT is applied to welded joints to mitigate the residual stresses, improve the metallurgical structure by tempering, and enhance the load-carrying capability of welded structures in service by reducing the likelihood of crack formation [14,15]. PWHT has been conducted according to industry codes and standards such as API 579RP [16] and ASME Division 2 [17]. Industry standards typically outline a consistent set of parameters, which include the application of spatially uniform heating below the lower transformation temperature (adjusted based on the steel grade or chemistry), specific heating rates, and prescribed isothermal holding or soaking times tailored to the thickness of the material/weld joint. It has been proven by recent experimental and numerical studies that PWHT-related codes could be excessively conservative, particularly for the soaking (holding) time in thick sections [18–21]. Finite element models were developed by Dong et al. [18] and Zhang et al. [20] verifying that sufficient residual stress reduction could be achieved with substantially reduced holding time, compared with the existing industry codes, as long as a reasonable PWHT temperature is employed. Experimental studies conducted by Chen et al. [19] and others [21,22] also confirm that stress relaxations predominantly occur during the ramping up with holding time having minor effects on the

* Corresponding author.
E-mail address: houman.amirabad@gmail.com (H. Alipooramirabad).

https://doi.org/10.1016/j.ijpvp.2025.105434
Received 19 September 2024; Received in revised form 16 December 2024; Accepted 5 January 2025
Available online 7 January 2025
0308-0161/

relieved residual stresses. There are, however, no experimental or numerical studies on the strain relief behaviour of Q&T steel welds during PWHT. This study reports the findings on strain relaxation time, for the first time, monitored during PWHT of Bisalloy 80 steel welds. The experiments were performed at the Australian Nuclear Science and Technology Organisation (ANSTO) using the KOWARI strain diffractometer. The data obtained from this experimental investigation offer a clear insight into the strain relaxation mechanism during PWHT of Bisalloy steel welds. This understanding could potentially lead to more economical and efficient PWHT time schedules.

Compliance with industry standards and regulations is essential for ensuring quality, safety, and reliability in engineering applications. However, there is a lack of comparative study with the current fitness-for-purpose approaches, R6 procedure [23] and BS 7910 [24] with regard to residual stress development during welding of Q&T steel. Both BS 7910 and R6 procedures provide guidelines and procedures for evaluating residual stresses as part of fitness for purpose assessment codes of practice [24]. This study aims to investigate the efficiency of PWHT in mitigating residual stresses in Bisalloy 80 steel welds via new in-situ and ex-situ neutron diffraction measurements and to compare the findings with the guidelines provided by the industry safety codes, BS7910 and R6.

2. Materials and methods

2.1. Base and filler material

Bisalloy Steel Group Limited (Wollongong, Australia) are the manufacturer of Q & T steels branded as Bisalloy grades. Bisalloy 80 (AS 3597-2008 GRADE 700) plate with the composition of Table 1 was used for the welding trial in the present investigation. The V-prepped steel plates with the thickness of 20 mm were cut into sections of 250 × 200 mm^2. These sections were then joined using the GMAW-P process with a total of 16 weld passes. The welded joint and geometry of the weld passes including different regions of the weld are shown by the optical macrographs in Fig. 1. Table 2 shows the summary of the welding parameters employed in this study.

Two identical welded samples were fabricated using the same welding parameters (i.e. filler material; sample heat input), one was used for the in-situ and ex-situ neutron diffraction analysis. The other was sectioned to obtain reference samples and used to measure the stress free lattice spacings (d0) at commensurate locations to the first full scale weld.

2.2. Stress-free sample preparation (d-zero) for in-situ and ex-situ neutron diffraction

The stress-free samples were prepared for both in-situ and ex-situ neutron diffraction measurements. Two different types of stress-free samples were prepared for Neutron Diffraction (ND) measurements, one for the in-situ and the other ex-situ and the details of the configuration is presented in Fig. 1. Both stress-free samples were cut from the fabricated sample, Fig. 1, by an Electrical Discharge Machine (EDM) having a wire diameter of 0.2 mm. The sample for in-situ neutron diffraction was prepared with the dimensions of 6 $mm \times 6\ mm \times 20\ mm$ while the dimensions of the sample for ex-situ neutron diffraction was 6 $mm \times 20\ mm \times 80\ mm$. It was shown that wire cutting of matchstick or reference samples from the area as mentioned above should induce full residual stress relaxation [21,25]. The lattice spacing measurements (d_0) for the stress-free samples were carried out on both the as-weld and PWHT specimens, employing identical measurement points corresponding to the regions examined for stressed specimens, within a gauge volume of 3 × 3 × 3 mm^3.

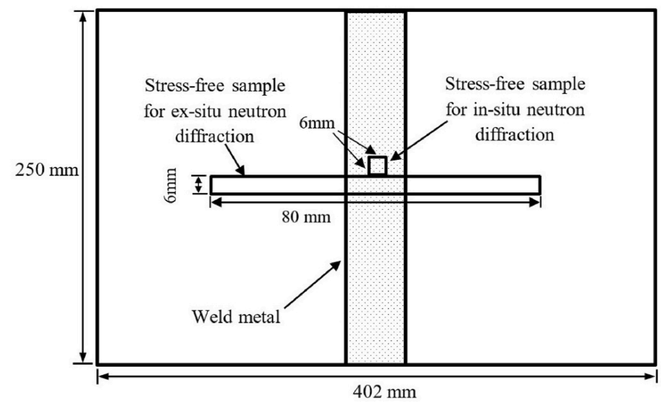

Fig. 1. Location of the stress-free samples for both in-situ and ex-situ neutron diffraction measurements.

Table 2
GMAW-P welding parameters and specifications.

Direction	Flat (1G)
Wire Diameter	1.2 mm
Electrode Class (AWS)	A5.28
Deposition Mode	GMAW-P (ISO 857 Process No.13)
Specification	ER 110S-G
Polarity	DC+
Shielding Gas	Ar 18 % Co2 (15–20 L/Minute)
Voltage	21–30 V
Current	135–225 A
Pre Heat Range	25 °C
Travel Speed	170–400 mm/min
Heat Input Range	0.48–2.19 kJ/mm

2.3. Ex-situ neutron diffraction (stress measurements prior-to and after PWHT)

The neutron diffraction method is a non-destructive, deep penetration scanning technique that generates three-dimensional strain maps within engineering components, unlike other techniques which are limited to surface and close-to-surface residual stress measurements [22,23]. Neutron diffraction (ND) measurements of residual strain/stress within the weld were conducted at ANSTO (Lucas Heights, Australia) using the KOWARI strain scanner diffractometer. The fundamental principle of the ND method for residual stress measurement is based on Bragg's law:

$$n\lambda = 2d \sin \theta \tag{1}$$

In this equation, θ represents the incident or reflection angle (also termed the Bragg angle, where 2θ is the measured angle of the neutron beam), λ is the wavelength of the incident neutron beam, d denotes the spacing between adjacent atomic planes within the crystal structure of

Table 1
Chemical analysis of Q&T Steel and consumable wire (% Weight).

	C	P	Mn	Si	S	Ni	Cr	Mo	Cu	Al	Sn	Ti	B	$CE_{(IIW)}$
Bisalloy 80	0.17	0.180	1.37	0.21	0.04	0.017	0.20	0.20	0.026	0.035	0.002	0.019	0.002	0.4812
Consumable wire	–	0.015	1.5	0.4	0.01	2.2	0.15	0.4	0.15	–	–	–	–	–

the tested material, and n is an integer specifying the order of the reflection plane (hkl).

The lattice strain, ε, is then calculated by measuring the stressed, (d_{hkl}), and stress-free, ($d_{hkl,0}$), inter-planer spacing as given in Equation (2).

$$\varepsilon_{hkl} = \frac{d_{hkl} - d_{hkl,0}}{d_{hkl,0}} \tag{2}$$

A monochromatic neutron beam provided by the monochromator Si (400) reflection with a wavelength of 1.67 Å was used to measure the scattering angle from the α-Fe (211) reflection. The nominal gauge volume was $3 \times 3 \times 3$ mm^3. Residual stress measurements were performed in three principal directions (longitudinal, transverse, and normal) across the weld at five different depths (3 mm, 6.5 mm, 10 mm, 13.5 mm and 17 mm) from the upper surface of the plate, as indicated on the transverse cross-section of the weld joint illustrated in Fig. 2.

Further details of experimentation and ND fundamentals can be found elsewhere [22,26,27].

2.4. In-situ neutron diffraction

Measurements were made every 60 s during PWHT to monitor strain relaxations at different stages of the heat treatment. Fig. 3 illustrates a schematic of the experimental setup, including a power source, heating blankets, six thermocouples (indicated as TCs) and d-zero samples attached to the back plate. ND was utilized alongside heating blankets wrapped around the welded plates to evaluate strain relaxations during PWHT of Bisalloy 80 steel welds. The heating was not standard as a gap of 35 mm was between the heating blankets to enable access for the neutron beam. Further details of the instrumentation (i.e. controllers and thermocouples) are provided in our previous reports and is not repeated here [21,22]. The heat treatment was performed at a 600 °C soaking temperature, with a ramp rate of 250 °C/h, and an isothermal holding time of 60 min. The heating blanket was switched off during cooling of the weld joint to the room temperature. The gauge volume of $3 \times 3 \times 3$ *mm* 3 was used for the in-situ ND strain measurements, similar to ex-situ ND, with a measurement time of 60s per point. In-situ ND during heat treatment was conducted in the single measurement point in the longitudinal direction with the highest residual stress magnitude (643 ± 28 MPa), as described in Section 3.2 (ex-situ measurements were done prior to PWHT on the same sample to determine this point and value). This point was located in the weld centreline, positioned 6.5 mm below the top surface of the plate. QKowari software, Kowari's in-house developed software, was utilized for the data analysis by fitting a Gaussian profile to the (211) reflection.

The evolution of d-spacing for the stress-free weld specimen (mechanically stress relieved through EDM cutting) was monitored as a function of time during PWHT. This is achieved through the measurement of d-spacing of the stress-relieved sample at several times during the heat, isothermal holding and cooling stages of the heat treatment. Measurement of the stress-free samples during the PWHT cycle is critical as it allows direct measurement ofthermal expansion and contraction. Note that the reference specimen (stress-free, d_0),was extracted in the middle of the weld where the in-situ ND strain measurements were conducted. Further details of experimentation (ex-situ and in-situ ND during PWHT) can be found in Refs. [21,22]. Fig. 4 outlines the various steps involved in the experiments (both in-situ and ex-situ ND) to provide further clarity on the experimental procedure.

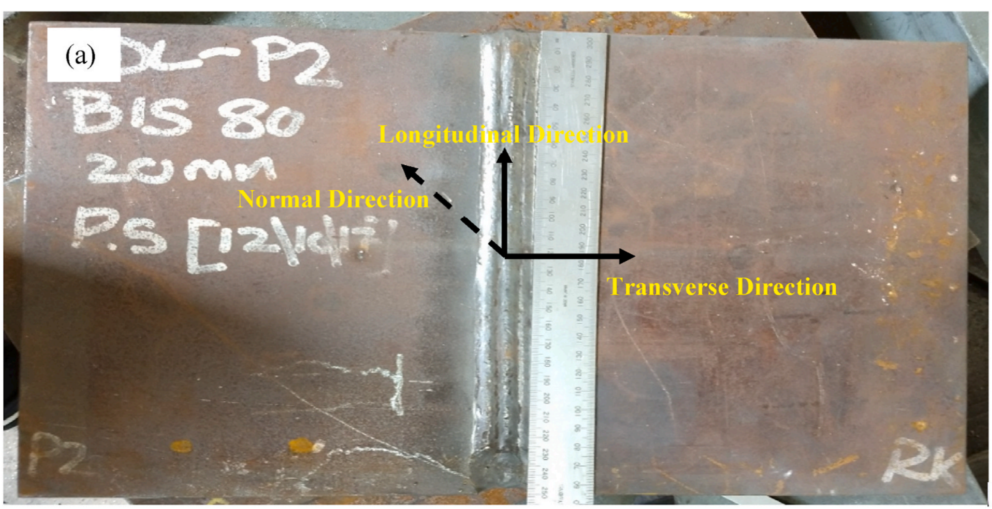

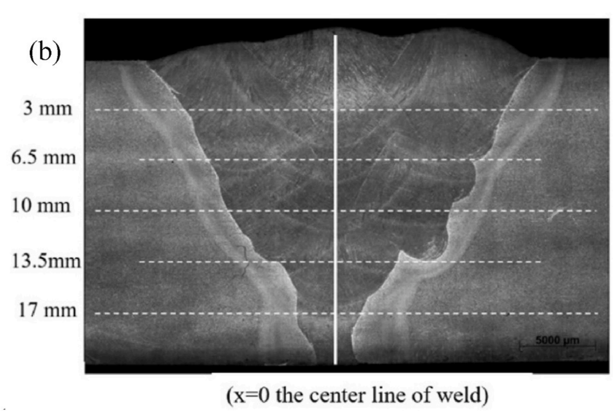

Fig. 2. Welding specimen and strain measurement directions (a) and the optical macrograph displays the weld joint, with dashed lines indicating the locations for neutron diffraction stress measurements (b).

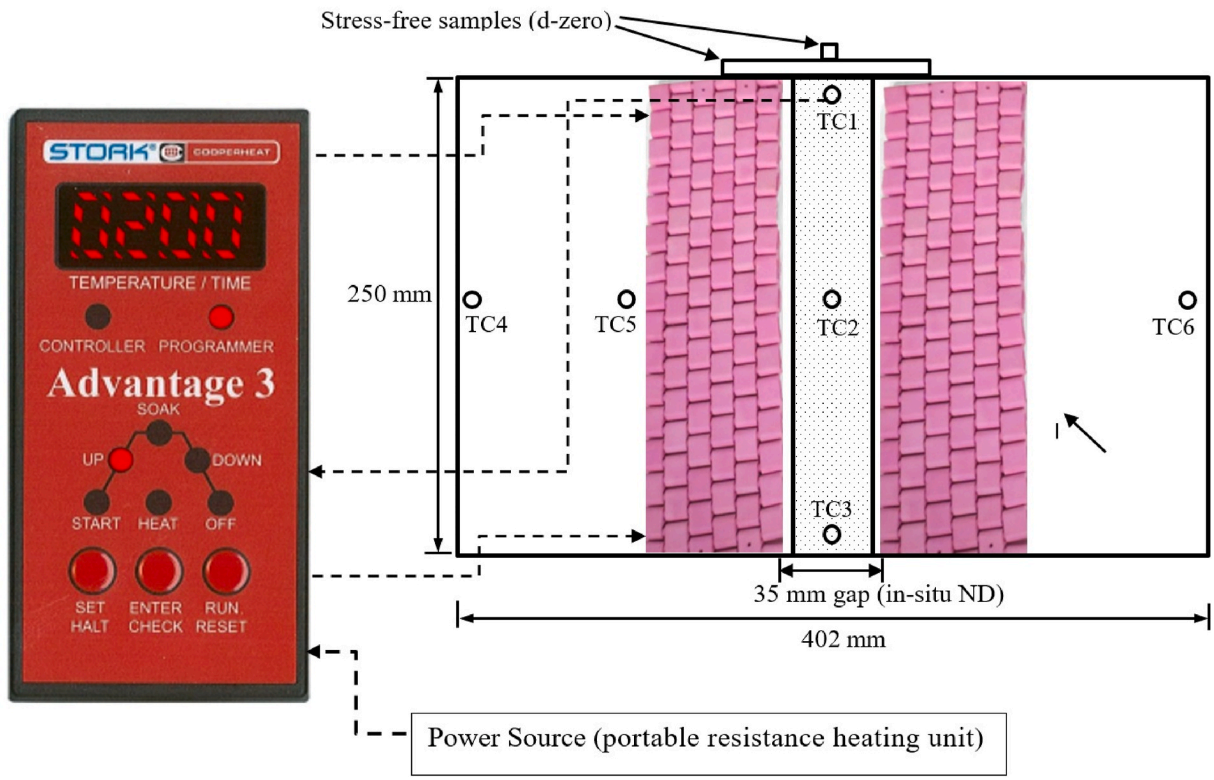

Fig. 3. Schematic of in-situ PWHT experimental set-up.

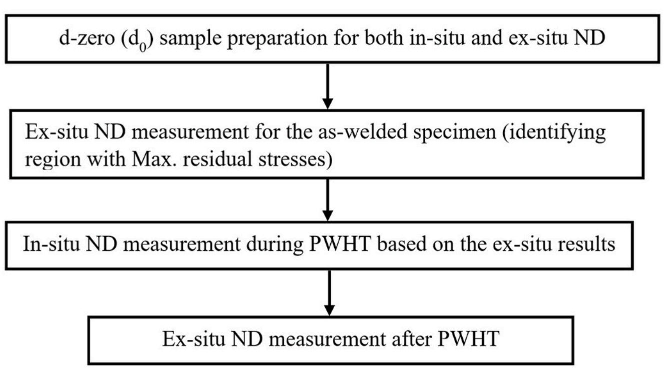

Fig. 4. Experimental procedure for sample preparation, both in-situ and ex-situ ND.

2.5. Code based residual stress estimation

A comparative analysis was conducted with two current industry standards, BS 7910 and R6 [24]. These industry standards provide information on residual stress distribution and magnitude for various materials and weld geometries. In the current investigation, residual stresses of a butt weld geometry in ferritic steel were analysed. The details of the comparative analysis are explained in the following sections.

2.5.1. BS 7910:2019

BS 7910:2019 is a fitness-for-service assessment code, serving as a “guide to methods for assessing the acceptability of flaws in metallic structures” [24]. BS 7910 standard provides an estimation of the longitudinal and transverse residual stresses in the weldments (Annex Q) [24]. It is stated that the longitudinal residual stress in the plate butt welds of ferritic steels is equal to the yield strength of the material at room temperature:

$$\frac{\sigma_R^L}{\sigma_Y} = 1 \tag{3}$$

Where σ_R^L is the longitudinal residual stress and σ_Y is the yield strength of the material:

($\sigma_Y = \max\left(\sigma_Y^P, \sigma_Y^W\right)$, σ_Y^P is the yield strength of the parent metal and σ_Y^W is the yield strength of the weld metal [24]. While, the transverse residual stress “should be assumed to be the lesser of the room temperature yield strength of the weld or parent material”.

The upper-bound through-thickness transverse residual stresses for the ferritic steels can be expressed as:

$$\frac{\sigma_R^T}{\sigma_Y} = 0.9415 - 0.0319\left(\frac{Z}{B}\right) - 8.3394\left(\frac{Z}{B}\right)^2 + 8.660\left(\frac{Z}{B}\right)^3 \tag{4}$$

Where σ_R^T is the transverse residual stress, Z is the depth in the parent metal and B is the thickness of the component. The BS7910 also provides guidelines for the residual stress distribution after PWHT and states that longitudinal stresses (stresses parallel to the weld) are equivalent to 30 % of the yield strength of the material in which the flaw is located. Transverse residual stresses after PWHT, on the other hand, are assumed to be equal to 20 % of the lesser of the yield strength of the parent or weld material.

2.5.2. Procedure R6

Procedure R6 utilises three approaches for the stress distribution of the as-welded components at room temperature including Level 1, Level 2 and Level 3. According to Level 1, which is a simple and conservative assessment, both the longitudinal and transverse residual stresses are in tensile mode and uniformly distributed within both the transverse and through-thickness directions having a magnitude equal to the material yield strength at room temperature [23]. Note that Level 1 is equivalent to the safety assessment procedure of BS 7910 and both of them are upper bound distributions and do not satisfy equilibrium.

For the R6-Level 2, two approaches are used to define residual stresses in butt welds, depending on the available information about welding conditions. In the case where residual stresses are known, Eqs. (3) and (4) can be used to provide residual stress distributions for the longitudinal direction. In the third approach, Level 3, estimation of the residual stress profile is based either on results obtained from available finite element (FE) -based parametric residual stress solution or experimentations [23,28].

If $r_o \leq t$, where t is a plate thickness (in mm), then:

$$r_0 = \sqrt{\frac{K}{\sigma_Y} * \frac{\eta q}{v}} \tag{5}$$

Where r_0 is the size of the plastic zone, q is the arc power ($q = V \times I$, V is the voltage and I is the current), K is the materials constant that depends on Young's modulus, density, specific heat of material, and coefficients of thermal expansion, σ_y is 0.2 % proof strength or yield strength of the parent metal, η is arc efficiency and v is the weld travel speed (in mm/s).

For the ferritic steels the provided values for $\eta = 0.8$ and $K = 153 \frac{Nmm}{J}$ [23,28].

For the thick materials, where $r_0 \leq t$ (t is the thickness of the plate), the following equation is used (y_0, which is measured in mm, and define the dimension of the plastic zone):

$$y_0 = \frac{1.033K}{\sigma_{YP}} * \frac{\eta q}{vt} \tag{6}$$

In the transverse direction for Level 2 (R6), the size of the plastic zone for the unrestrained and restrained plates are t and 2t, respectively. Fig. 5 presents a schematic comparison of BS 7910 and R6 Level 2 profiles for surface residual stress, while Fig. 6 shows the comparison for the through-thickness residual stress.

The through-thickness longitudinal residual stress distributions for both codes (BS7910 and R6) are equal to the yield stress of the weld metal. While a polynomial function (Eq. (5)) is used to determine the through-thickness transverse residual stress profile for the R6-Level 2 code.

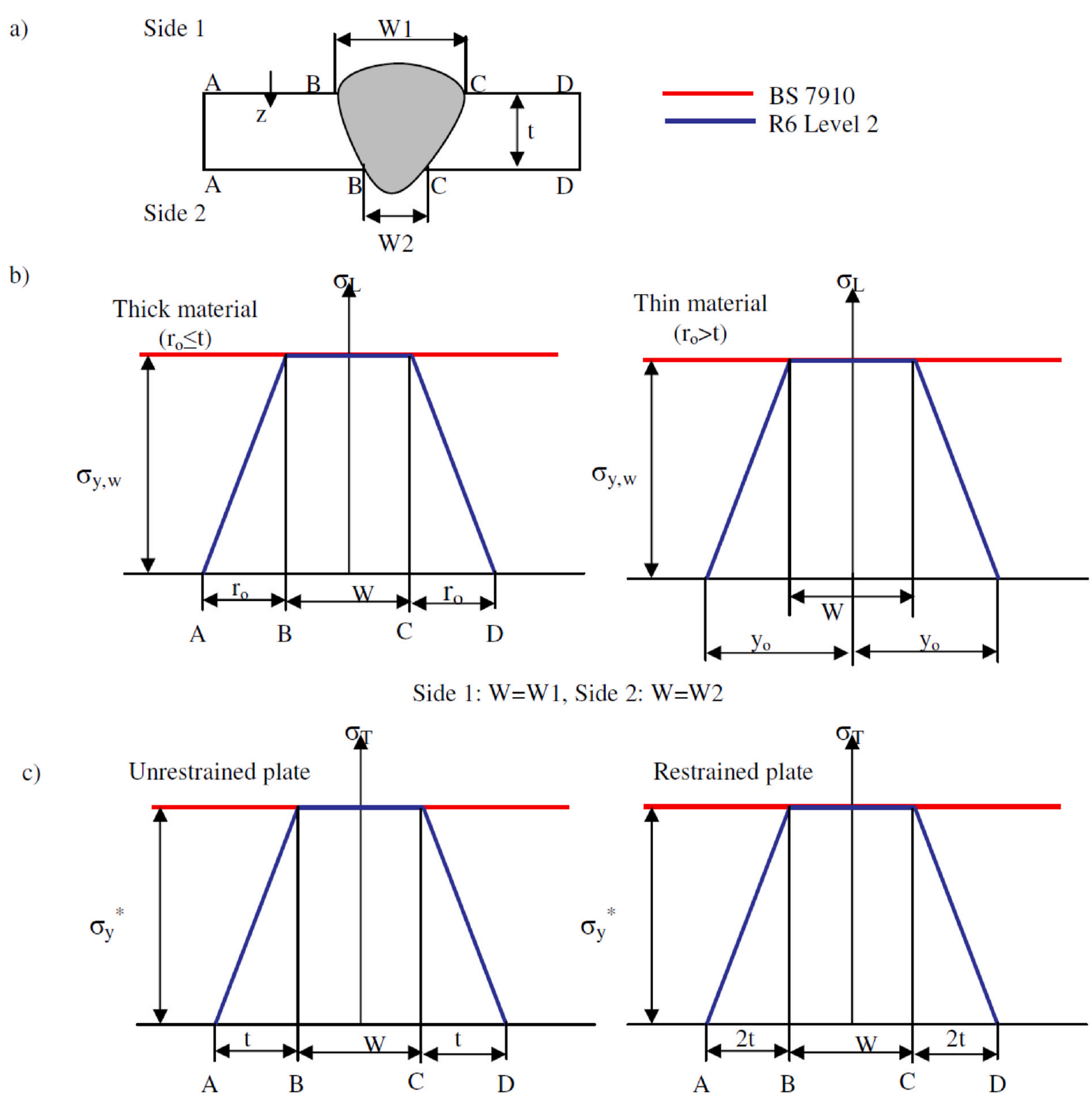

Fig. 5. Residual stress distributions with R6 Level 2 and BS 7910 codes for a ferritic butt weld in the schematic cross-section (a) longitudinal (b), and transverse (c) directions (W is the width of the weld) [23].

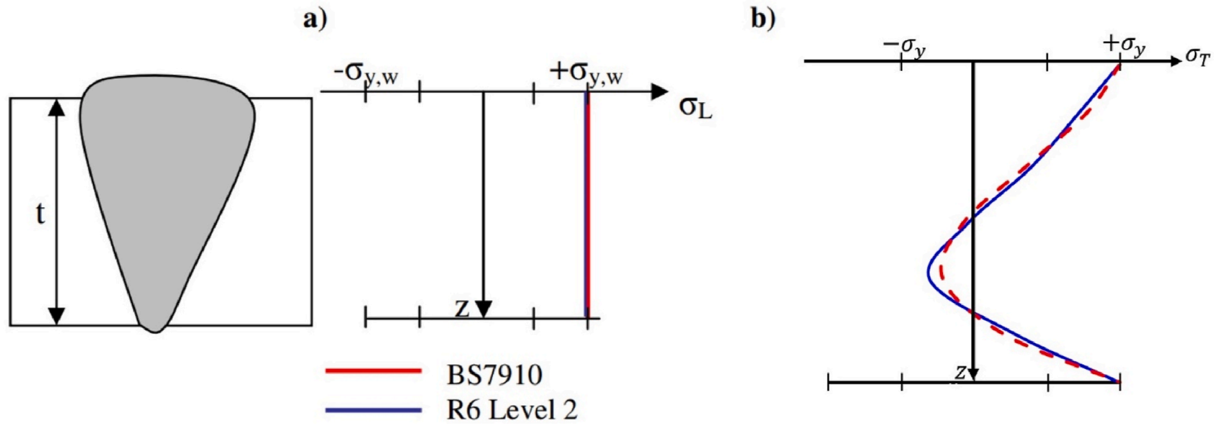

Fig. 6. Comparison of through-thickness residual stress distributions with R6 Level 2 and BS 7910 codes for (a) longitudinal and (b) transverse directions [23,24].

$$\sigma_T \Big/ \sigma_y(z/t) = 1 - 0.917(z/t) - 14.533(z/t)^2 + 83.115(z/t)^3 - 215.45(z/t)^4 + 244.16(z/t)^5 - 96.36(z/t)^6 \tag{7}$$

3. Results and discussion

3.1. Ex-situ neutron diffraction measurements

Residual stress measurements were conducted at 92 locations for the welded sample prior-to and after PWHT. The contour maps were created to provide the residual stress distribution across the weld, as shown in Figures (7-8). The measurement positions are highlighted with the black cross markers on the contour plots, while the broken lines represent the boundaries between different zones of parent metal (PM), heat affected zone (HAZ) and weld metal (WM). The residual stress in the longitudinal direction is predominantly tensile in the WM and HAZ but become compressive further away from the HAZ. Lower residual stresses are evident in both transverse and normal directions, in comparison with longitudinal stresses, in the WM and HAZ of the as-welded specimen. The highest magnitude of residual stress was found in longitudinal direction at the depth of 6.5 mm below the surface, 3 mm away from the

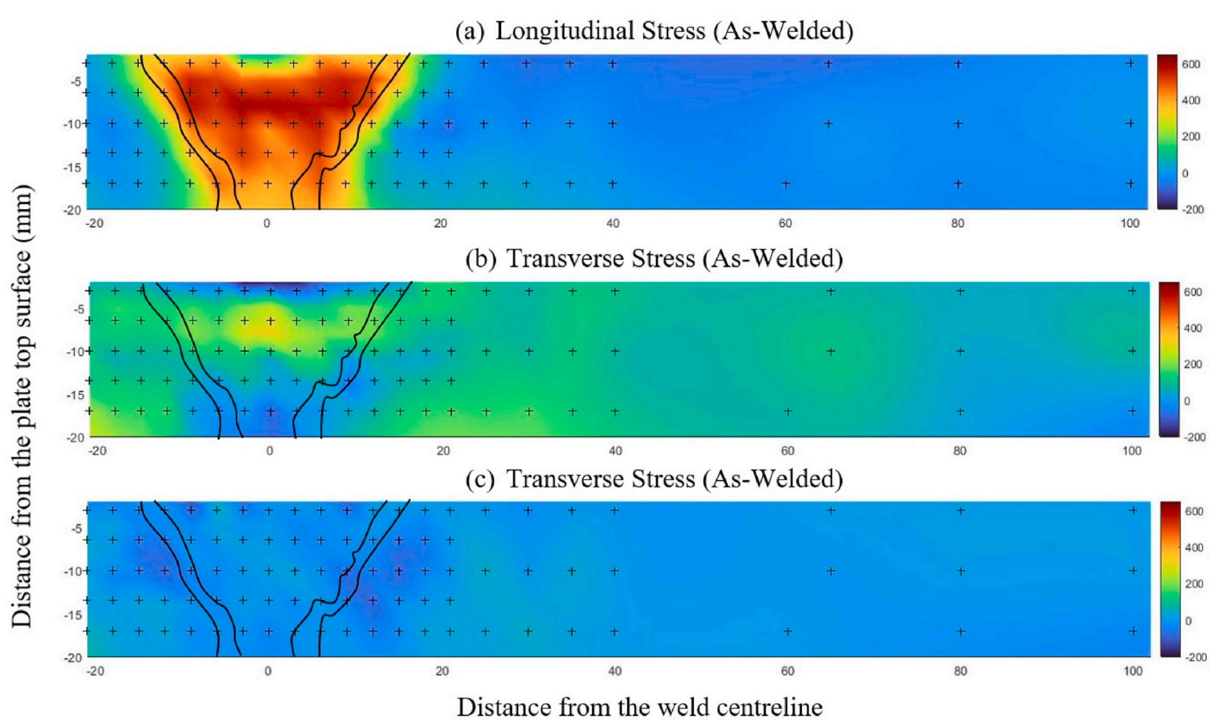

Fig. 7. Contour maps of the residual stress distribution for the as-welded specimen in (a) longitudinal, (b) transverse and (c) normal, directions (x-and y-axis in mm & stress scale in MPa).

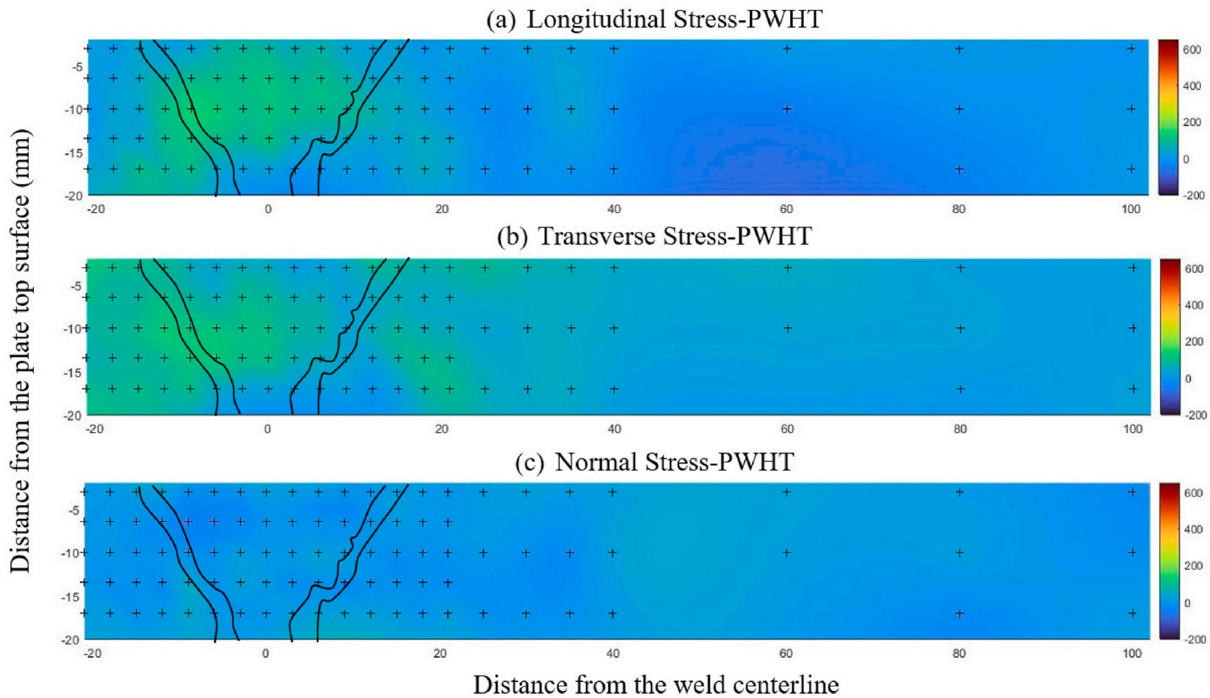

Fig. 8. Contour maps of the residual stress distribution for the heat-treated specimen in (a) longitudinal, (b) transverse and (c) normal directions.

weld centreline (Fig. 7a) reaching a peak value of 646 ± 16 MPa, which is almost equal to the yield strength of the WM. This is the position chosen for the later in-situ measurements. This region is associated with the upper weld passes with minimal tempering effects. The tempering effect on the residual stress relief is more pronounced for the initial passes up to the mid-plate thickness, where the heat applied during deposition of the later weld passes tempers the previous passes (Fig. 7a-c).

Following PWHT, a significant reduction in residual stresses is noted. Specifically, in the longitudinal direction, the maximum residual stress magnitude reduces to approximately 145 ± 15 MPa (Fig. 8a). This value represents approximately 23 % of the yield strength of the weld metal (WM), with yield strengths of the parent metal (PM) and weld metal (WM) being 650 and 710 MPa, respectively [11]. This also confirms the success of the implemented heat treatment in reducing the residual stresses within the welded joint.

3.2. In-situ neutron diffraction measurements

Neutron diffraction was utilized to evaluate the relaxations of the residual strains during PWHT for the highly stressed region (6.5 mm below the top surface and 3 mm away from the weld centreline) of the as-welded joint.

As previously discussed, the evolution of the interplanar spacing (d_0) in the stress-free sample during the PWHT program was observed to differentiate between the stress relief changes in the bulk sample and those attributed to thermal expansion. The measured d_0 data during PWHT is plotted in Fig. 9 indicating a linear relationship with temperature.

The linear regression fit was therefore applied to calculate d_0 values corresponding to the respective temperatures according to the following equation (Eq. (7)):

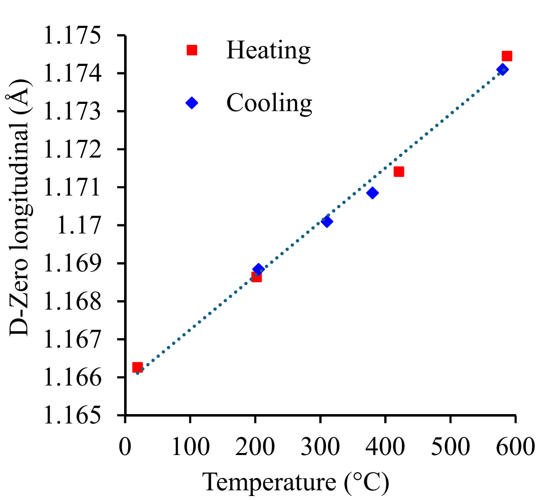

Fig. 9. Longitudinal stress-free measurements of lattice parameter during PWHT.

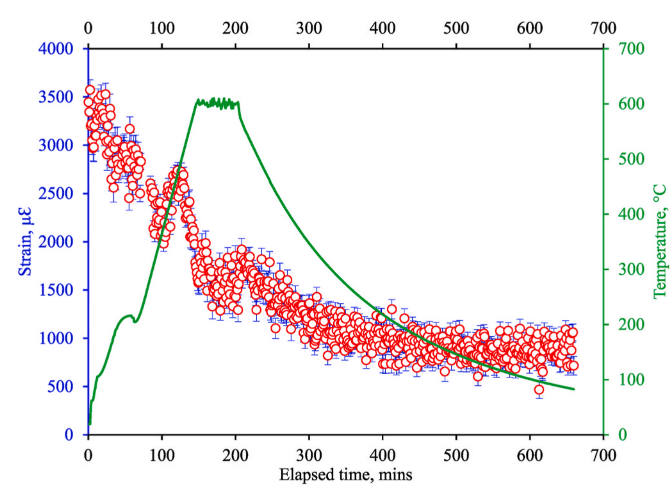

Fig. 10. Longitudinal residual strain relaxation with the corresponding temperature during the PWHT cycle (the measurement location is 6.5 mm below the plate top surface, 3 mm away from the weld centerline).

$$d_0(T) = mT + c \tag{8}$$

Where both "m" and "c" are constants and extracted from the linear regression fit of the data and T is the temperature (°C). The resulting strain was then calculated using the "d_0'' value obtained from Eq. (7) as indicated in Eq. (8) below;

$$\varepsilon_{xx}(T) = \frac{d_{xx}(T) - d_0(T)}{d_0(T)} \tag{9}$$

During PWHT a substantial reduction in the longitudinal residual strains were observed during the reheating stage up to 600 °C (Fig. 10). The strain at the beginning of the reheating stage was about 3500 ± 90 με dropping to the value of 1800 ± 138 με at the beginning of the isothermal holding time at 600°C. A significantly higher rate of strain relaxation was observed during the reheating stage in comparison with the holding time; ~800 με/h for reheating vs ~250 με/h for holding time. The total relaxed strain during isothermal soaking was therefore 250 ± 125με. Note that the residual strains at the end of the cooling stage were about 950 ± 110 με (~%25 of the initial strain) which agrees with the ex-situ residual stress measurements after PWHT (Fig. 8).

The data indicate that strain relaxation predominantly took place during the reheating phase to the soaking temperature (~67 %) and the contribution of the holding time reduces the strain by a smaller amount (~10 % relaxation). This finding is consistent with the authors' previously published work for the high strength low alloy steel welds, API 5L X70, where the soaking time was found to be less significant for the strain relaxation (~13 % of the total relaxed strains) during PWHT [21, 22]. A high strain relaxation during reheating, from 450°C to 600 °C, which is followed by the linear stress relief during the holding stage may be an indication that creep (primary and secondary) is responsible for the strain relaxation during PWHT. This observation is also in line with the author's previous studies on the microstructural changes which occur after PWHT where rearrangement of dislocations and formation of sub-grains through polygonization in the HAZ and WM of the heat-treated joints was reported for the high-strength low-alloy [11,21] and Bisalloy 80 [11] steel welds. Interestingly, the data trend line is in very good agreement with the numerical investigation conducted by Dong et al. [18] where a linear residual stress reduction in the early stage of heat treatment can be seen which can be associated with the linear reduction in yield strength of the WM. Then a rapid reduction in the residual strains at a temperature range between 450 °C and 600 °C can be seen which is due to rapid creep strain development. Also, minimal strain relaxation occurs during the holding stage as a result of insignificant creep strain change during holding time.

Similar observations were also made by numerical [29] and experimental studies [19,30] where a minimal rate of strain relaxation in the early stage (yield strength reduction), followed by a high rate of strain relaxation and eventually linear stress relief was reported for different weldments confirming that creep-type strain-induced relief is responsible for the strain relaxations during PWHT.

3.3. Comparison with BS7910 and R6 procedure

The results of experimental measurement of residual stresses of the weld joint were compared with BS 7910:2019 and R6 procedure. Comparing neutron diffraction residual stress measurements to fitness-for-purpose standards bridges the gap between advanced experimental techniques and practical engineering applications. To enable comparison between two sets of data, the measured residual stress values were normalized (Normalized Residual Stress or NRS) to the material yield stress of both the weld metal (weld region) and parent metal (outside of the weld zone). The graphs in Fig. 11 show the comparative analysis for the ND residual stress distributions for the as-welded sample (3 mm below the weld surface, across the weld), together with the estimates of BS 7910 and R6. Both codes overestimate the residual stresses, particularly BS7910:2019. The highest magnitude of the residual stress in

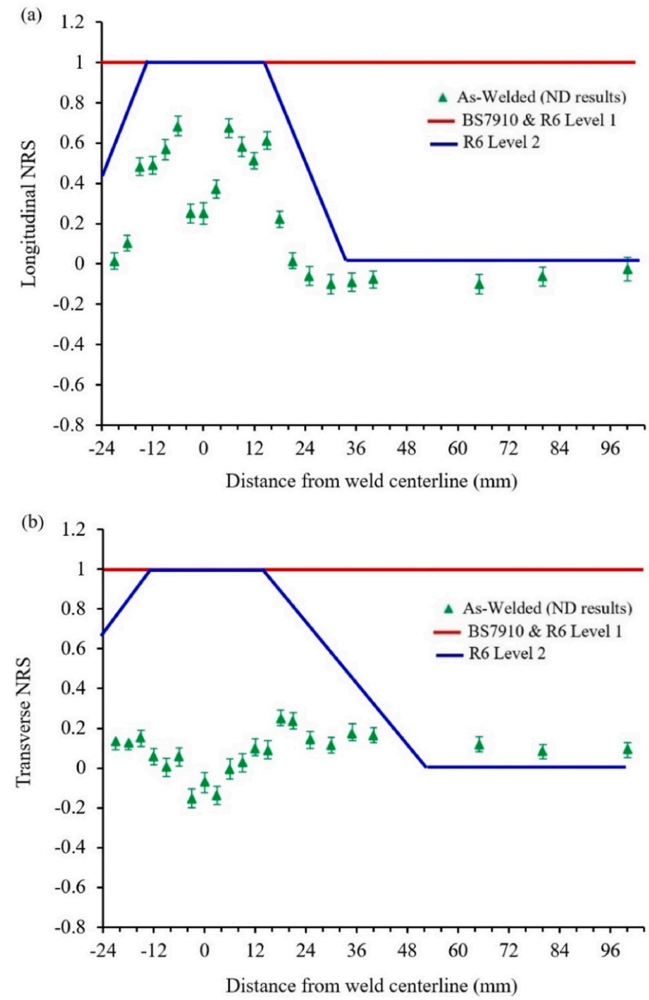

Fig. 11. Comparison of Normalized residual stress (NRS) distributions between experimental neutron diffraction (ND) and fitness for purpose assessments (BS7910 & R6) procedures for across the surface of the weld in as-welded conditions for (a) longitudinal and (b) transverse directions.

longitudinal and transverse directions were about 0.70 and 0.25 times of the yield strength of the weld metal, respectively. Interestingly, the data trend for the longitudinal direction is matched well with R6 level 2 (see Fig. 11a), though the normalized residual stresses were lower than those of the code.

Fig. 12 compares through-thickness distributions for the as-welded sample at the weld centreline (x = 0 mm) with the BS 7910 and R6 approaches and a previous experimental investigation conducted by Paradowska et al. [28]. The highest magnitude of the residual stress in the longitudinal direction is at 6.5 mm depth of the plate which is equal to the yield strength of the material at room temperature which is consistent with both industry codes. However, through-thickness transverse residual stress is underestimated in both codes. The highest magnitude of residual stress in the transverse direction, through-thickness, is about 0.65 times the yield strength of the material and is located at the depth of 6.5 mm of the plate (higher than both industry codes). Comparing the present results with the measured results of Paradowska et al. [28], the normalized through-thickness residual stresses in both directions show strong agreement in data trend and a very close match of the two data sets. It also shows that the through-thickness transverse residual stresses were underestimated in both cases in comparison with the fitness-for-purpose approach of R6 level 2 and BS7910 -2019. The findings have strong industry implications and could be incorporated into fitness-for-purpose assessment

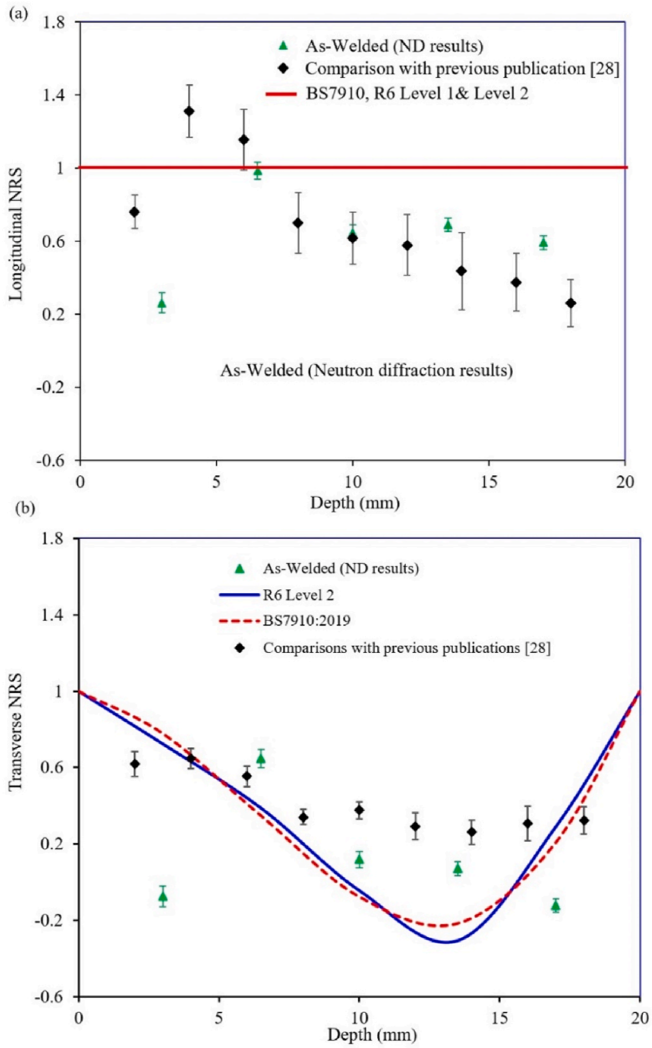

Fig. 12. Comparison between the through-thickness NRS distribution for the as-welded sample for (a) longitudinal and (b) transverse directions (x = 0 the weld centerline, as shown in Fig. 2).

codes and refine the results, particularly for the cases where residual stresses are underestimated (i.e. through-thickness transverse residual stress in the as-welded sample).

4. Conclusions

This study monitored the residual strain relaxation behaviour of the Q&T steel welds during PWHT. ND measurements were used to measure residual strains before, during, and after PWHT. The key findings were:

1) High tensile residual stresses were seen in the as-welded specimens (the maximum of 646 MPa which is about 91 % of the yield strength of the WM) but significantly reduced after PWHT (~145 MPa, about 23 % of the yield strength of the WM).
2) Approximately 67 % of strain relaxation occurred during the reheating phase, with only ~10 % occurring during the isothermal holding at 600 °C. This highlights the importance of the reheating rate as a critical process parameter for optimizing PWHT.
3) The minimal strain relaxation in the early stage of heat treatment is due to plastic strain effects which is followed by a high rate of strain relief due to creep strain development which occurs far earlier than the component reaching the isothermal holding temperature.
4) Both BS7910 and R6 procedures provided conservative estimates for longitudinal and transverse residual stresses near the weld toe but underestimated through-thickness transverse residual stresses. Notably, transverse residual stress fields, across the surface of the weld, showed significant overestimations in the fitness-for-purpose assessments by both standards. However, the transverse residual stress profiles observed in this study closely align with those reported in published literature, suggesting the need for refinement in these assessment codes.
5) The study's findings offer unique and valuable data to support finite element modelling of this complex process. By combining experimental insights with finite element simulations, the study provides a framework for optimizing the Post-Weld Heat Treatment (PWHT) process, particularly focusing on the reheating phase, leading to considerable cost savings in industrial applications.

CRediT authorship contribution statement

Houman Alipooramirabad: Writing – original draft, Visualization, Validation, Methodology, Investigation, Formal analysis, Data curation, Conceptualization. **Anna Paradowska:** Writing – review & editing, Validation, Software, Resources, Project administration, Funding acquisition, Data curation. **Mark Reid:** Software, Resources, Investigation, Data curation. **Reza Ghomashchi:** Writing – review & editing, Supervision, Resources, Project administration, Investigation, Funding acquisition.

Ethical Approval

Not applicable.

Funding

This research was supported by the Australian Nuclear Science and Technology (ANSTO) under the facilities access award P7087.

Declaration of competing interest

The authors declare that they have no known competing financial interests or personal relationships that could have appeared to influence the work reported in this paper.

Acknowledgment

The neutron diffraction analysis was conducted using the Kowari strain scanner at ANSTO under the facilities access award P7087. Welding activities were carried out at Australian Welding Solutions (AWS) and the Mechanical Engineering Workshop at the University of Adelaide. We gratefully acknowledge the support of Neville Cornish (AWS) for providing access to welding facilities and Pascal Symons (University of Adelaide) for performing the welding at both AWS and the University of Adelaide.

Data availability

Data will be made available on request.

References

[1] H.M. Clark, R.J. Llewellyn, Assessment of the erosion resistance of steels used for slurry handling and transport in mineral processing applications, Wear 250 (2001) 32–44.
[2] M. Balakrishnan, V. Balasubramanian, G.M. Reddy, Effect of joint design on ballistic performance of quenched and tempered steel welded joints, Mater. Des. 54 (2014) 616–623.
[3] S. Ryan, H.J. Li, M. Edgerton, D. Gallardy, S.J. Cimpoeru, Ballistic Evaluation of an Australian Ultra-high Hardness Steel, 2016.

[4] H. Alipooramirabad, N. Cornish, R. Kurji, A. Roccisano, R. Ghomashchi, Quenched and tempered steels welded structures: modified Gas Metal Arc welding-pulse vs. Shielded Metal Arc welding, Metals 13 (5) (2023) 887.
[5] G. Magudeeswaran, V. Balasubramanian, G.M. Reddy, T.S. Balasubramanian, Effect of welding processes and consumables on tensile and impact properties of high strength quenched and tempered steel joints, J. Iron Steel Res. Int. 15 (2008) 87–94.
[6] G. Magudeeswaran, V. Balasubramanian, G.M. Reddy, Hydrogen induced cold cracking studies on armour grade high strength, quenched and tempered steel weldments, Int. J. Hydrogen Energy 33 (2008) 1897–1908.
[7] T. Falkenreck, A. Kromm, T. Böllinghaus, Investigation of physically simulated weld HAZ and CCT diagram of HSLA armour steel, Weld. World 62 (2018) 47–54.
[8] F. Hochhauser, W. Ernst, R. Rauch, R. Vallant, N. Enzinger, Influence of the soft zone on the strength of welded modern HSLA steels, Weld. World 56 (2012) 77–85.
[9] B. Hanhold, S.S. Babu, G. Cola, Investigation of heat affected zone softening in armour steels Part 1–Phase transformation kinetics, Sci. Technol. Weld. Join. 18 (2013) 247–252.
[10] B. Hanhold, S.S. Babu, G. Cola, Investigation of heat affected zone softening in armour steels Part 2–Mechanical and microstructure heterogeneity, Sci. Technol. Weld. Join. 18 (2013) 253–260.
[11] H. Alipooramirabad, A. Paradowska, M. Reid, R. Ghomashchi, Effects of PWHT on the residual stress and microstructure of Bisalloy 80 steel welds, Metals 12 (2022), https://doi.org/10.3390/met12101569.
[12] V.S. Raja, T. Shoji, Stress Corrosion Cracking: Theory and Practice, Elsevier, 2011.
[13] H.C. Ma, Z.Y. Liu, C.W. Du, H.R. Wang, X.G. Li, D.W. Zhang, Z.Y. Cui, Stress corrosion cracking of E690 steel as a welded joint in a simulated marine atmosphere containing sulphur dioxide, Corrosion Sci. 100 (2015) 627–641.
[14] D. Kaplan, G. Murry, Thermal, metallurgical and mechanical phenomena in the heat affected zone, Metall. Mech. Weld. Process. Ind. Appl. (2008) 89–131.
[15] M.S. Zhao, S.P. Chiew, C.K. Lee, Post weld heat treatment for high strength steel welded connections, J. Constr. Steel Res. 122 (2016) 167–177, https://doi.org/10.1016/j.jcsr.2016.03.015.
[16] A.P.I. Standard, 579-1/ASME FFS-1 Fitness for Service, Inst, Houston, TX Am. Pet, 2007.
[17] A. Boiler, P.V. Code, Edition: ASME Section VIII Division 2, Rules Constr, Press. Vessel. Altern. Rules, 2015.
[18] P. Dong, S. Song, J. Zhang, Analysis of residual stress relief mechanisms in post-weld heat treatment, Int. J. Pres. Ves. Pip. 122 (2014) 6–14.
[19] B. Chen, A. Skouras, Y.Q. Wang, J.F. Kelleher, S.Y. Zhang, D.J. Smith, P.E. J. Flewitt, M.J. Pavier, In situ neutron diffraction measurement of residual stress relaxation in a welded steel pipe during heat treatment, Mater. Sci. Eng. 590 (2014) 374–383.
[20] J. Zhang, P. Dong, S. Song, Stress relaxation behavior in PWHT of welded components, in: Press. Vessel, Pip. Conf., 2011, pp. 673–679.
[21] H. Alipooramirabad, A. Paradowska, M. Reid, R. Ghomashchi, Effect of holding time on strain relaxation in high-strength low-alloy steel welds: an in-situ neutron diffraction approach, J. Manuf. Process. 73 (2022) 326–339, https://doi.org/10.1016/j.jmapro.2021.11.005.
[22] H. Alipooramirabad, A. Paradowska, O. Lavigne, R. Ghomashchi, M. Reid, In situ neutron diffraction measurement of strain relaxation in welds during heat treatment, Sci. Technol. Weld. Join. 22 (2017) 484–495.
[23] A.M. Paradowska, J.W.H. Price, T.R. Finlayson, R.B. Rogge, R.L. Donaberger, R. Ibrahim, Comparison of neutron diffraction residual stress measurements of steel welded repairs with current fitness-for-purpose assessments, in: ASME Press. Vessel, Pip. Conf., 2008, pp. 603–612.
[24] B. Standard, Guide to methods for assessing the acceptability of flaw in metallic structures, BS 7910, London, Br. Stand. Inst. 2 (2019) 15.
[25] T. Roy, A. Paradowska, R. Abrahams, M. Law, P. Mutton, M. Soodi, W. Yan, Residual stress in laser cladded heavy-haul rails investigated by neutron diffraction, J. Mater. Process. Technol. 278 (2020) 116511.
[26] A.J. Allen, M.T. Hutchings, C.G. Windsor, C. Andreani, Neutron diffraction methods for the study of residual stress fields, Adv. Phys. 34 (1985) 445–473.
[27] H. Alipooramirabad, A.M. Paradowska, R. Ghomashchi, A. Kotousov, N. Hoye, Prediction of welding stresses in WIC test and its application in pipelines, Mater. Sci. Technol. 32 (2016) 1462–1470.
[28] A.M. Paradowska, J.W.H. Price, T.R. Finlayson, R.B. Rogge, R.L. Donaberger, R. Ibrahim, Comparison of Neutron Diffraction Measurements of Residual Stress of Steel Butt Welds with Current Fitness-For-Purpose Assessments, vol. 132, J. Press. Vessel Technol., 2010.
[29] H. Takazawa, N. Yanagida, Effect of creep constitutive equation on simulated stress mitigation behavior of alloy steel pipe during post-weld heat treatment, Int. J. Pres. Ves. Pip. 117 (2014) 42–48.
[30] J. Rolph, A. Evans, A. Paradowska, M. Hofmann, M. Hardy, M. Preuss, Stress relaxation through ageing heat treatment–a comparison between in situ and ex situ neutron diffraction techniques, Compt. Rendus Phys. 13 (2012) 307–315.